JOURNAL OF MATERIALS SCIENCE 27 (1992) 4097–4106

Thermo-elastic stress analysis to predict design parameters of continuous casting

A. A. I. MANESH
Arkansas Center for Technology Transfer, University of Arkansas, Fayetteville, AR 72701, USA

The continuous casting process is superior to conventional casting in several ways, including more uniform production, energy savings, higher productivity and foremost the ability to cast to a form that is directly rolled on finishing mills. Characteristics of the process, including solidification time of minutes versus hours for ingot casting and high stress development in the solidifying shell, are discussed. A generalized approach to modelling heat transfer, solidification and stress distribution in continuous casting were developed. Illustrated models of this application include a simulation of the casting process with a view towards predicting temperature ranges, stress distributions and the effects of the operating parameters. The ratio of maximum applied stress to yield stress is used as a basis to predict the location of the bending rollers and the radius of the curved portion. This stress ratio provides design engineers with a tool for predicting effective parameters on a continuous casting machine for new installation design.

1. Introduction

The superiority of the continuous casting method in primary metal production has been recognized for over a century. The advantages of this process include a substantial increase in yield, more uniform production, energy savings and higher productivity. The greatest benefit of continuous casting is the ability to bypass conventional ingot casting and hence cast to a form that is directly rolled on finishing mills. Continuous casting usually follows this sequence of operations:

1. delivery of the liquid metal into the casting mould;
2. formation of the cast section in the water-cooled mould;
3. withdrawal of the casting from the mould with pinch rollers;
4. removal of heat from the casting by water spray or water-bath immersion to complete the solidification;
5. cutting and removal of the cast bars.

A schematic diagram showing the main components of a continuous casting machine is presented in Fig. 1. Several commercial arrangements for continuous casting are presently available. The types of continuous casting machines include vertical, vertical with bending, arc with straight mould, arc with curved mould and horizontal. Fig. 2 contains the principal example types of these machines. The vertical continuous casting machine was originally the major choice for steel production. The vertical with bending and the curved ingot machines, although more complicated in construction, were developed to minimize machine height and allow installation in existing plants without crane height modification [1].

The use of this process, for any machine type, results in increased yield, improved surface condition, and upgraded internal quality of the product. In order to reach this goal, two sets of coupled parameters must have predictable effects and controllable values. These parameters are thermal (controls solidification process) and mechanical (controls production). For simplicity, the thermal model is assumed to decouple from the mechanical system. This means the heat transfer model calculates the temperature distribution first and then imposes a thermal load on the mechanical system.

2. Thermal parameters and heat transfer in continuous casting

The thermal aspects of solidification are complex because they involve several parameters. The temperature-dependent thermal properties of the solidifying metal, the latent heat release due to the solidification process, the gap formation and heat transfer within the mould, the heat removal by spray cooling water, and the speed of casting are a few of the parameters involved. The rate of heat extraction and solidification in continuous casting is relatively fast. The solidification time is measured in minutes compared to hours for conventional casting. The ingot created by the continuous casting encounters three entirely different cooling environments of mould, spray and radiation. As a result, the cast is subjected to very steep temperature gradients which can cause serious thermal stress problems. Over the years, many analytical and numerical models have been developed and employed to help optimize the operating thermal parameters within continuous casting. By using various assumptions, the process has been modelled in one dimension [2], two dimensions [3, 4], or three dimensions [5, 6].

0022–2461

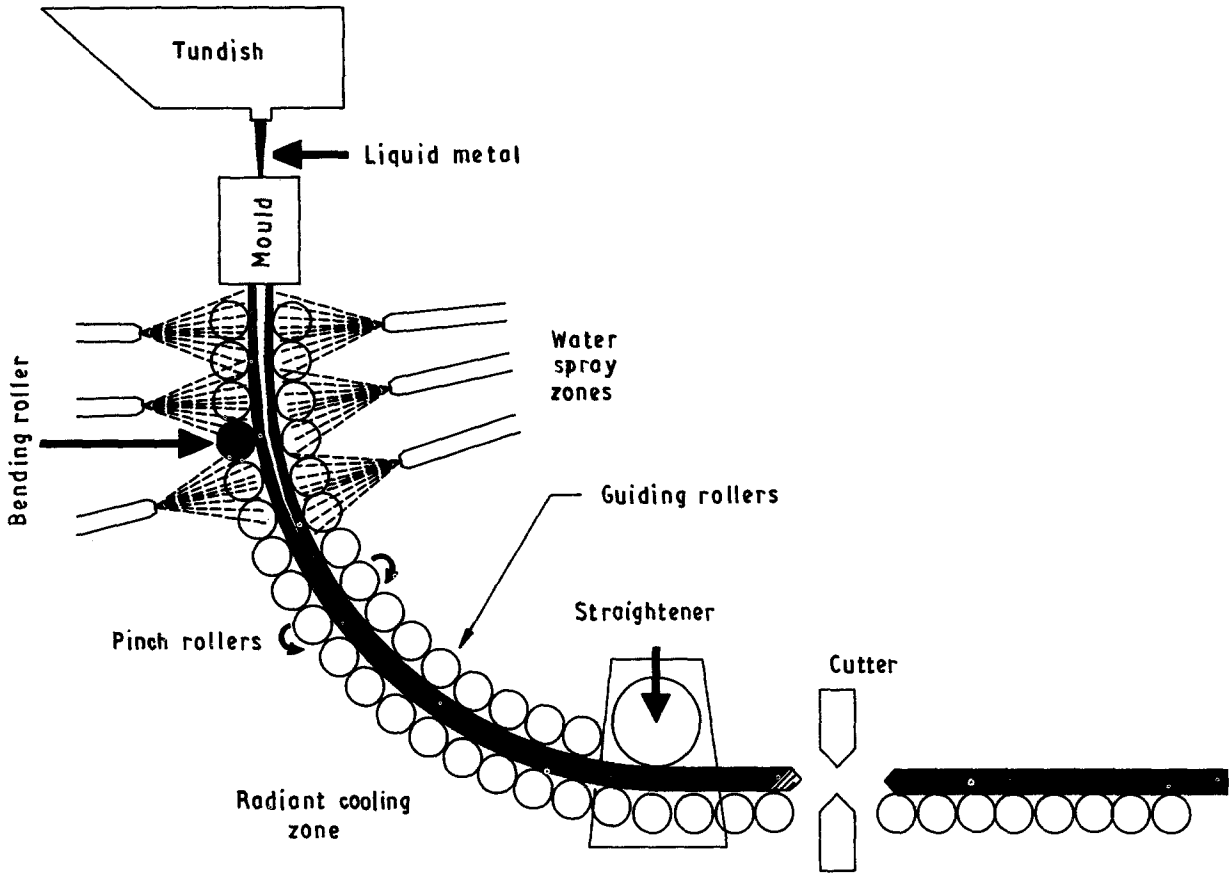

Figure 1 Section view of a continuous casting installation.

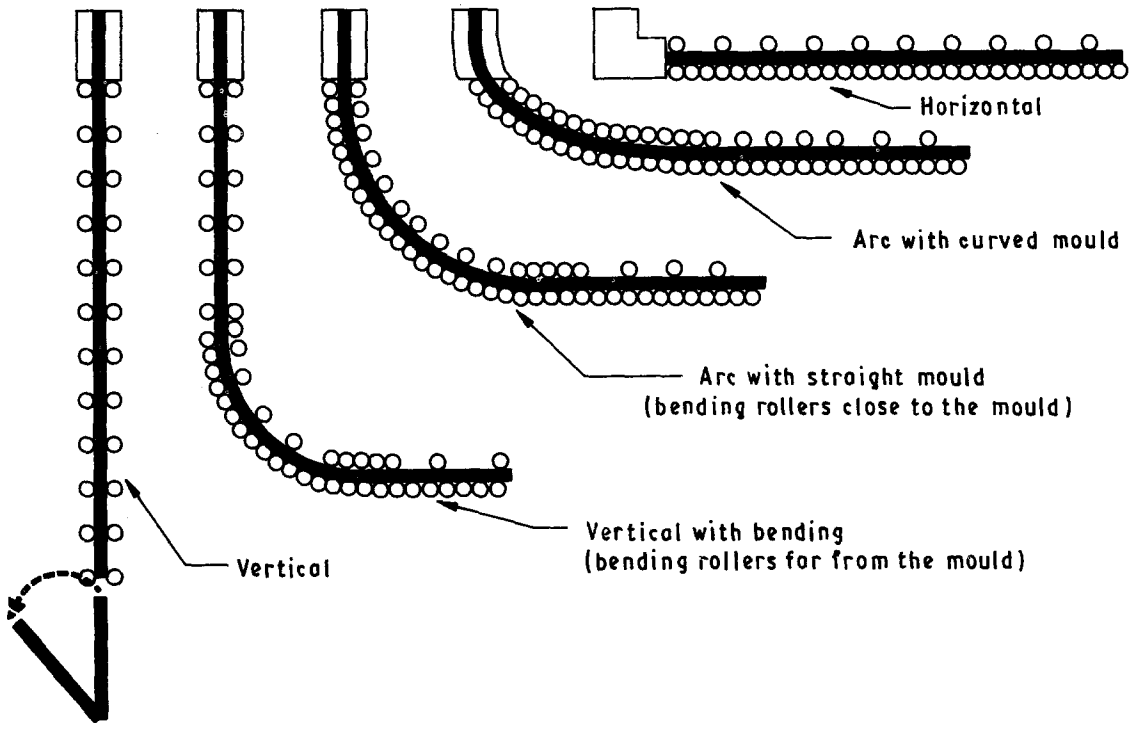

Figure 2 Principal types of continuous casting.

2.1. Finite element formulation for heat transfer

The differential equation of heat flow, expressed in the rectangular coordinates (x, y, z) and referenced to a fixed origin in the solid, is known by

$$\partial/\partial x(K_{xx}\partial T/\partial x) + \partial/\partial y(K_{yy}\partial T/\partial y) + \partial/\partial z(K_{zz}\partial T/\partial z) = PC_p\partial T/\partial t \quad (1)$$

The coefficients K_{xx}, K_{yy} and K_{zz} are thermal con-

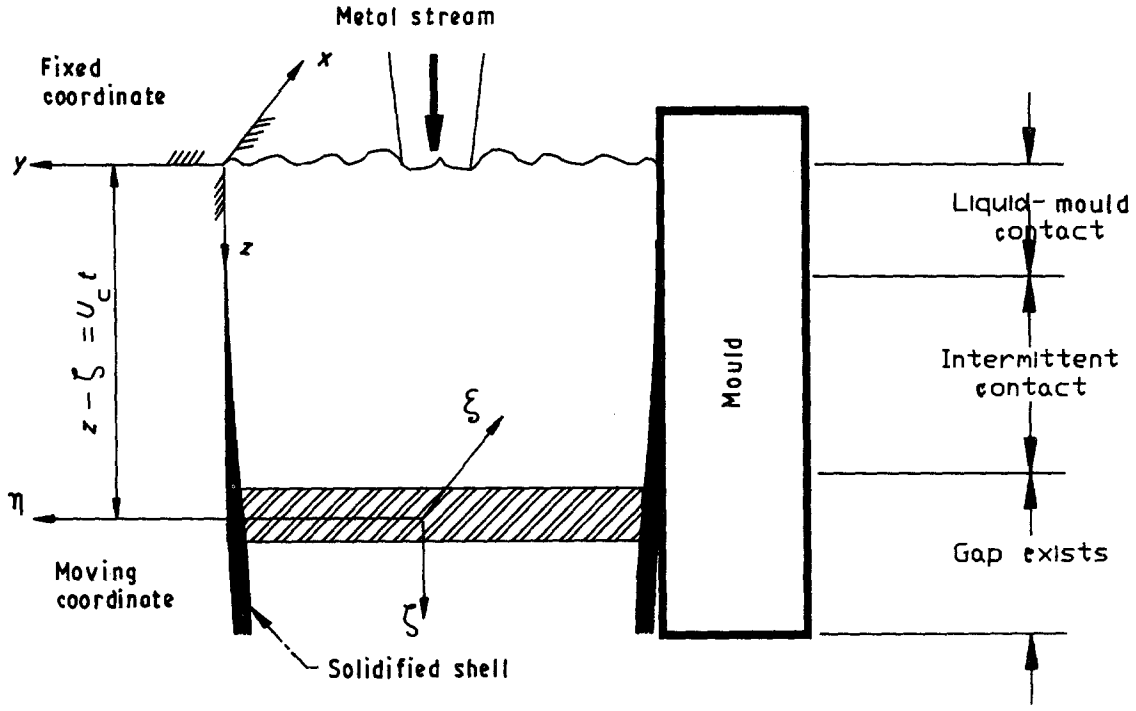

Figure 3 Mould boundary.

ductivity in x, y and z directions, resp., C_p is the specific heat, and P is density.

Assume the fixed origin is attached to the mould and that a second coordinate system is attached on the casting surface, as shown in Fig. 3. The second coordinate is moved away from the fixed origin with the casting velocity, U_c (cm s^{-1}). The (x, y, z) coordinate is attached to the mould, where the alloy is liquid and the (ξ, η, ζ) coordinate is connected to the cast ingot in the casting direction of z or ζ. The temperature in the new moving origin will be defined as $T = f(\xi, \eta, \zeta, t')$ where t' is time measured in the moving coordinate. Fig. 3 depicts the moving coordinate

$$z - \zeta = U_c t \tag{2a}$$

or

$$\zeta = z - U_c t \tag{2b}$$

and

$$\partial\zeta/\partial z = 1 \tag{3a}$$

$$\partial\zeta/\partial t = -U_c \tag{3b}$$

$$\partial t'/\partial t = 1 \tag{3c}$$

so

$$\partial T/\partial t = [(\partial T/\partial\zeta)(\partial\zeta/\partial t)] + [(\partial T/\partial t')(\partial t'/\partial t)] \tag{4a}$$

or

$$\partial T/\partial t = -U_c \partial T/\partial\zeta + \partial T/\partial t' \tag{4b}$$

and also

$$\partial T/\partial x = \partial T/\partial\xi \tag{5a}$$

$$\partial T/\partial y = \partial T/\partial\eta \tag{5b}$$

$$\partial T/\partial z = \partial T/\partial\zeta \tag{5c}$$

After substitution into Equation 1

$$\partial/\partial\xi(K_{xx}\partial T/\partial\xi) + \partial/\partial_\eta(K_{yy}\partial T/\partial\eta) + \partial/\partial\zeta(K_{zz}\partial T/\partial\zeta) = PC_p(\partial T/\partial t' - U_c\partial T/\partial\zeta) \tag{6a}$$

or, in the general form,

$$\nabla(K\nabla T) = -U_c PC_p \partial T/\partial\rho\zeta + PC_p \partial T/\partial t' \tag{6b}$$

in a quasi-stationary state $\partial T/\partial t' = 0$. Changing the notation yields the governing equation

$$\partial/\partial x(K_{xx}\partial T/\partial x) + \partial/\partial y(K_{yy}\partial T/\partial y) + \partial/\partial z(K_{zz}\partial T/\partial z) + U_c PC_p \partial T/\partial z = 0 \tag{7}$$

By assuming $K_{xx} = K_{yy} = K_{zz} = K$, the governing differential equation reduces to

$$\partial/\partial x(K\partial T/\partial x) + \partial/\partial y(K\partial T/\partial y) + \partial/\partial z(K\partial T/\partial z) + U_c PC_p \partial T/\partial z = 0 \tag{8}$$

The finite element equations can be obtained using a variational approach or Galerkin's method. The element stiffness matrix, [ESM], and the element force vector, {EF}, are [7]

$$[\mathrm{ESM}] = \int_{-1}^{1}\int_{-1}^{1}\int_{-1}^{1} [B(\xi,\eta,\zeta)]^T [D] \times [B(\xi,\eta,\zeta)] |\det[J]| \, d\xi \, d\eta \, d\zeta + \int_{-1}^{1}\int_{-1}^{1}\int_{-1}^{1} U_c C_p P [N(\xi,\eta,\zeta)]^T \{\partial N_i/\partial\zeta\} \times |\det[J]| \, d\xi \, d\eta \, d\zeta + \int_{-1}^{1}\int_{-1}^{1} h[N(\xi,\eta)]^T [N(\xi,\eta)] |\det[J]| \, d\xi \, d\eta \tag{9}$$

and

$$\{\mathrm{EF}\} = \int_{-1}^{1}\int_{-1}^{1} hT_{\mathrm{inf}} [N(\xi,\eta)]^T |\det[J]| \, d\xi \, d\eta \tag{10}$$

where N is a matrix involving the shape functions, B is related to the derivatives of the shape functions, D is conduction matrix and J is the Jacobean matrix of

transformation. Also, h is the heat transfer coefficient and T_{inf} is the ambient temperature.

For the three-points Gaussian quadrature, twenty-seven integration points are required to integrate numerically the volume integral. The quadrature form of Equation 9 is

$$[ESM] = \sum_{l=1}^{3}\sum_{j=1}^{3}\sum_{k=1}^{3}[f_1(\xi_i, \eta_j, \zeta_k)H_{ijk} + U_c PC_p f_2(\xi_i, \eta_j, \zeta_k)H_{ijk}]|\det[J]| + \sum_{l=1}^{3}\sum_{j=1}^{3}[f_3(\eta_j, \zeta_k)H_{jk}]\det[J] \quad (11)$$

where

$$f_1(\xi_i, \eta_j, \zeta_k) = [B]^T[D][B] \quad (12)$$

$$f_2(\xi_i, \eta_j, \zeta_k) = U_c PC_p[N]^T\{\partial N/\partial\zeta\} \quad (13)$$

and

$$f_3(\xi_j, \eta_k) = h[N]^T[N] \quad (14)$$

and H_{ijk} is the weighing coefficient.

The quadrature form of Equation 10 is

$$\{EF\} = \sum_{i=1}^{3}\sum_{j=1}^{3}[f_4(\pm 1, \eta_i, \zeta_j)H_{ij}]|\det[J]| \quad (15)$$

where

$$f_4(\pm 1, \eta_i, \zeta_j) = hT_{inf}[N]^T \quad (16)$$

The temperature at any given point in an element can be calculated using

$$T = \sum_{i=1}^{20} T_i N_i \quad (17)$$

where T_i is the nodal temperature, N_i is the shape function for a given element evaluated at the point for which the temperature is needed, and i is the number of nodes in the element.

2.2. Boundary conditions

Three different types of boundary conditions, as shown in Fig. 1, occur when Equation 8 is applied to a continuous casting ingot. At time zero, the temperature profile of the mould slice is equal to the incoming molten metal temperature. The centre surface boundary conditions of

$$\partial T/\partial x = 0 \quad (18a)$$

and

$$\partial T/\partial y = 0 \quad (18b)$$

result from the assumption of symmetrical heat transfer from all edges of the casting. The surface boundary conditions are varied as indicated in Fig. 1 to represent the three types of cooling processes (mould, spray, and radiation).

The first and most important zone of cooling is in the mould. The heat flux from the solidifying steel to the mould cooling water is largely determined by the size of the gap between the mould and the solidified shell. The best way to consider this situation is by modelling the ingot and the mould, both to compute the temperature distribution and to calculate the gap thickness due to shrinkage [8]. Fig. 3 shows that the molten materials, from the inlet to the place of solid shell formation, are in direct contact with the mould. In this region, the liquid metal is separated from the mould by a thin layer of lubricant. Below this region a solidified shell forms and tries to pull away from the mould wall, but the ferrostatic pressure forces the casting surface to have intermittent contact with the mould. Finally, as the solidified shell gains enough strength, it pulls the casting away from the mould wall forming a large gap. In this zone, the heat transfer takes place by radiation and conduction through the gas in the gap. The total resistance to the heat flow in the zones with direct contact and intermittent contact is [9]

$$U_{good} = U_{lub} + \frac{x_{mould}}{K_{mould}} + \frac{1}{h_{water}} \quad (19)$$

where X_{mould} and K_{mould} are the mould wall thickness and the thermal conductivity, respectively, and h_{water} is the heat transfer coefficient of mould cooling water. The heat-transfer coefficient of the mould cooling water is represented by h_{water}. In the zone where the gap exists, the thermal resistance from the solidified shell to the mould cooling water is

$$U_{gap} = \frac{1}{(K_{gap}/X_{gap}) + \Sigma_s E_e(T^4 - T_m^4)} + U_{good} \quad (20)$$

where K_{gap} and X_{gap} are the conductivity of the gas in the gap and the gap thickness. Σ_s is the Stefan Boltzmann constant (5.672×10^{-12} W cm^{-2}) and E_e is the emissivity. The casting surface and mould surface temperatures are T and T_m respectively.

Cooling the ingot, once it has left the mould, consists in one or more stages of spray and heat loss through radiation. The heat-transfer coefficient for the spray boundary was determined experimentally by Mizikar [10]. The coefficient can be modelled as

$$q_s = h_s(T - T_w) \quad (21)$$

where h_s is the spray heat-transfer coefficient, T is the casting surface temperature and T_w is the spray cooling water temperature.

The heat transfer in radiation cooling is

$$q = h_{rad}(T - T_{inf}) \quad (22)$$

where the effective heat-transfer coefficient for radiation is h_{rad}

$$h_{rad} = \Sigma_s E_e(T^2 + T_{inf}^2)(T + T_{inf}) \quad (23)$$

where T is the casting surface temperature and T_{inf} is the surrounding temperature.

2.3. Material properties

Heat conduction in continuous casting includes phase changes. During the solidification process there exists a solid front, a liquid front, and a transition zone between these where the latent heat is absorbed. The specific heat was modified to account for the release of the latent heat of fusion, in the transition zone of the ingot during solidification [11], Fig. 4.

The thermal conductivity of the ingot, at temperatures above liquidation, were modified to account for

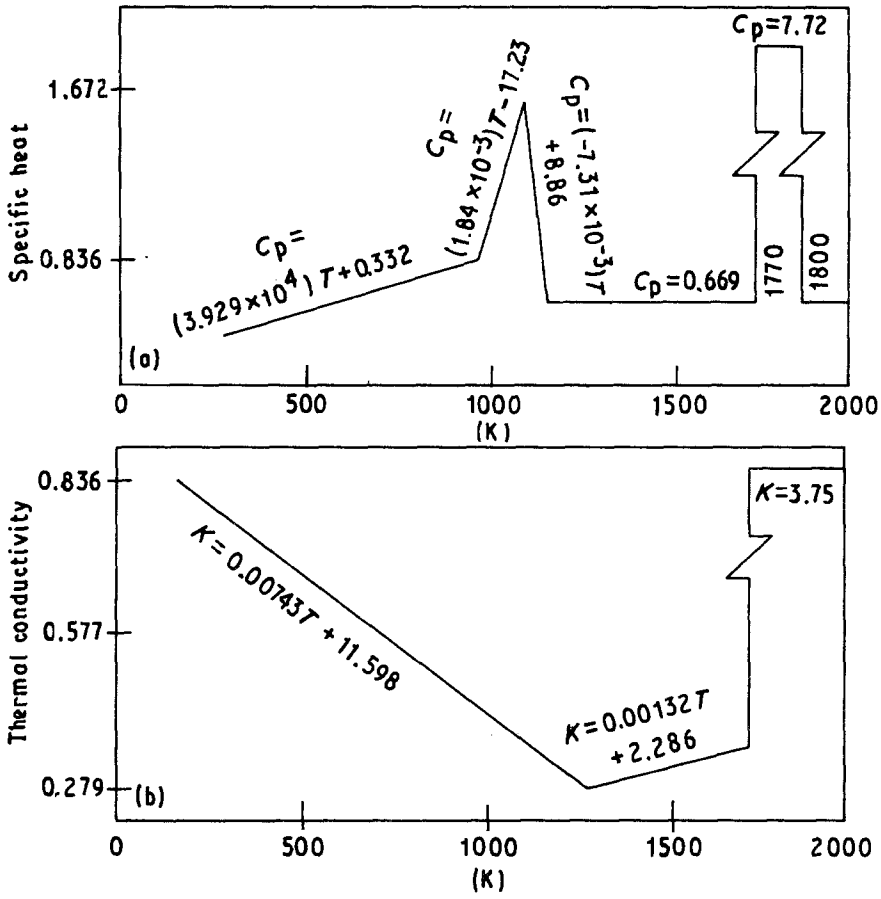

Figure 4 Material properties. (a) Modified specific heat. (b) Modified thermal conductivity.

the effects of the convection current in the molten core. The thermal conductivity value of molten steel was multiplied by a factor of ten [12]. The variations in thermal conductivity from room temperature to the steel formation temperature are depicted in Fig. 4.

3. Mechanical parameters and stress field in continuous casting

High stress, arising from forces acting internally and externally upon the ingot, develops in the solidifying shell during continuous casting. Internal forces may result from the expansion or contraction of the shell due to sudden temperature changes. For example, rapid reheating of the surface can occur immediately below the mould or spray zones and may cause tensile stress to be produced near the solidification front. External force examples are the application of the pinch rollers (which pull ingots off the mould), misalignment of the guide rollers (to direct the ingot), the bending and straightening rollers (which force the ingot to change direction), and mould oscillation (to prevent sticking). In addition, the ferrostatic pressure inside the solidified shell applies a load which can cause bulging if the distance between the guide rollers is large.

Whatever their origins, the stresses can have a deleterious effect both on the casting operation and upon the quality of the cast product. If the stresses are sufficiently high and tensile in nature they can lead to the formation of a variety of surface and internal cracks. Surface cracks are the most serious type of cracking problem because they are not reweldable and must be removed before rolling. Internal cracks, if they are near the solidification front, are a lesser problem in this regard because they have a good chance to be rewelded before complete solidification. The internal cracks which are between the outer surface and solidification front (mid-way cracks) must be rewelded fully to yield a completely sound rolled product.

3.1. Finite element formulation for stress analysis

A three-dimensional finite element formulation for elasticity was used. The displacement values were obtained by assuming a displacement field and then minimizing the potential energy. The important requirement of this theorem is that the selected displacement equations must satisfy the displacement boundary conditions [11]. A 20-node brick element with 60 degrees of freedom was used in calculating the stress field developed in the solidified shell.

3.2. Boundary conditions

3.2.1. Thermal load

Because the thermal model is assumed to be decoupled from the mechanical system, the temperature field is first calculated and then imposed as a thermal load on the mechanical system.

3.2.2. Internal forces

(a) Ferrostatic pressure which produces stress in the solidifying skin must be examined, along with any casting shrinkage. As the casting shrinks from the

mould the ferrostatic pressure tends to bulge the casting until contact with the mould is restored. The casting develops both bending and membrane stresses as a result of the bulging. Once the casting exits from the mould there is no longer a continuous restraint to bulging. If the guide rollers are too widely spaced, bulging might occur to the extent that the casting tears, ruptures, or becomes too large to pass through the guide rollers.

(b) Gravity force is the weight of the casting which contributes axial stress to the skin. The unsupported weight of the cast below any specified level would be resisted completely by the axial tension in the cast above that level, without the outside influence of the drive rollers.

3.2.3. External forces

(a) Mould friction force is produced when continuous casting moulds are oscillated to prevent "welding" or "sticking" of the cast metal to the mould. This oscillation produces a highly apparent friction in the solidified skin. This friction force is dependent upon the coefficient of friction and the normal force due to ferrostatic pressure. The friction coefficient is contingent upon the mould surface roughness, mould material, and type of lubricant used. Owing to the lack of information regarding the magnitude of the friction coefficient, the friction force was assumed to be equal and in the opposite direction of the force used by the drive rollers plus the unsupported weight of the ingot.

(b) A tractive force is exerted by the drive rollers which can counteract or add to the gravity force. If the tractive effort of the drive rollers tends to draw the casting, then the effective axial tensile force at a specific point is the weight of the casting below this point plus the tractive effort. If the tractive effort of the drive rollers tends to compress or distort the casting, then the effective axial force is the weight minus the tractive effort.

(c) The guiding roller's friction forces are not important in the straight vertical section due to the clearance between the rollers and the casting. These rollers are important in the curved section because most of the weight of the casting is carried by the rollers. The friction forces on the roller depend upon the space between the rollers, the roller bearing's friction coefficient and the presence of any tears in the casting. The friction force resulting from the rollers was ignored due to a lack of information on its value. The contact point between the guide rollers and the casting creates a set of zero displacements in the direction perpendicular to the casting direction.

(d) Bending and straightening rollers at the beginning and end of the curved portion force the casting to be displaced in the direction of the radius of curvature. Bending and straightening rollers provide a known displacement, the magnitude is radius dependent, on the ingot. The displacement direction is towards the centre of the curved portion.

3.3. Material properties

Young's modulus was assumed to vary linearly with temperatures according to a relationship given by Grill *et al.* [13]

$$E = 1.08 \times 10^6 - 1030(T - T_{tr}) \quad \text{kg cm}^{-3} \qquad (24)$$

for temperatures in excess of 800 °C where T_{tr} is the A3 transformation temperature.

The strain limit of elasticity was also assumed to be temperature dependent [13]

$$E_{el} = 1.47 \times 10^4 - (8.00 \times 10^8)T \quad \text{for } T > 1100\,^{\circ}\text{C} \qquad (25)$$

$$E_{el} = 4.84 \times 10^4 - (3.68 \times 10^7)T \quad \text{for } T < 1100\,^{\circ}\text{C} \qquad (26)$$

Poisson's ratio was assumed to be constant because it is insensitive to temperature: $\nu = 0.33$.

4. Computer programming

The commercially available common finite element packages are not suitable for this analysis because the thermal conductivity and specific heat are temperature dependent. In order to solve the equations, a two part computer program was generated to calculate the nodal temperature, displacements, stress field, yield stress, and ratio of calculated stress to yield stress.

The first part of the computer program analyses heat transfer. This portion of the program has the capability to assume an initial temperature distribution for the casting, calculate the element stiffness matrix and calculate the element force vector. Then the program assembles the information into a system of equations, solves the system of equations for the nodal temperature values, and finally compares the nodal temperature with the assumed temperature. If the maximum difference between the temperature at any single node is less than 5 K, the program will write the nodal temperature and route it to the stress analysis routines; otherwise, the program will replace the old assumed temperature values by the new calculated values and then repeat the calculations. The results are presented in Fig. 5.

The second part of the computer program utilizes the three-dimensional finite element elasticity formulations to analyse the stress within the casting. This portion of the program initially reads the temperature distribution and boundary conditions. By using the brick elements with 20 nodes, it then calculates the stiffness matrix and force vector to solve for the nodal displacements. The last step is to evaluate the Von-Mises stress and then calculate the ratio of the Von-Mises stress to the yield stress. Yield stress at any temperature is calculated by multiplying Young's modulus and the strain limit of elasticity. The Von-Mises stress is defined as $(3J_2)^{1/2}$, where J_2 is the second stress in the variants

$$J_2 = [1/2(S_x^2 + S_y^2 + S_z^2) + T_{xy}^2 + T_{xz}^2 + T_{yz}^2]^{1/2} \qquad (27)$$

where $S_x = S_{xx} - S_m$, $S_y = S_{yy} - S_m$, $S_z = S_{zz} - S_m$, and $S_m = 1/3(S_{xx} + S_{yy} + S_{zz})$. Calculating absolutely correct stress values is difficult, due to the uncertainty resulting from the assumed mechanical properties, the presumed external forces and the inherent complexity

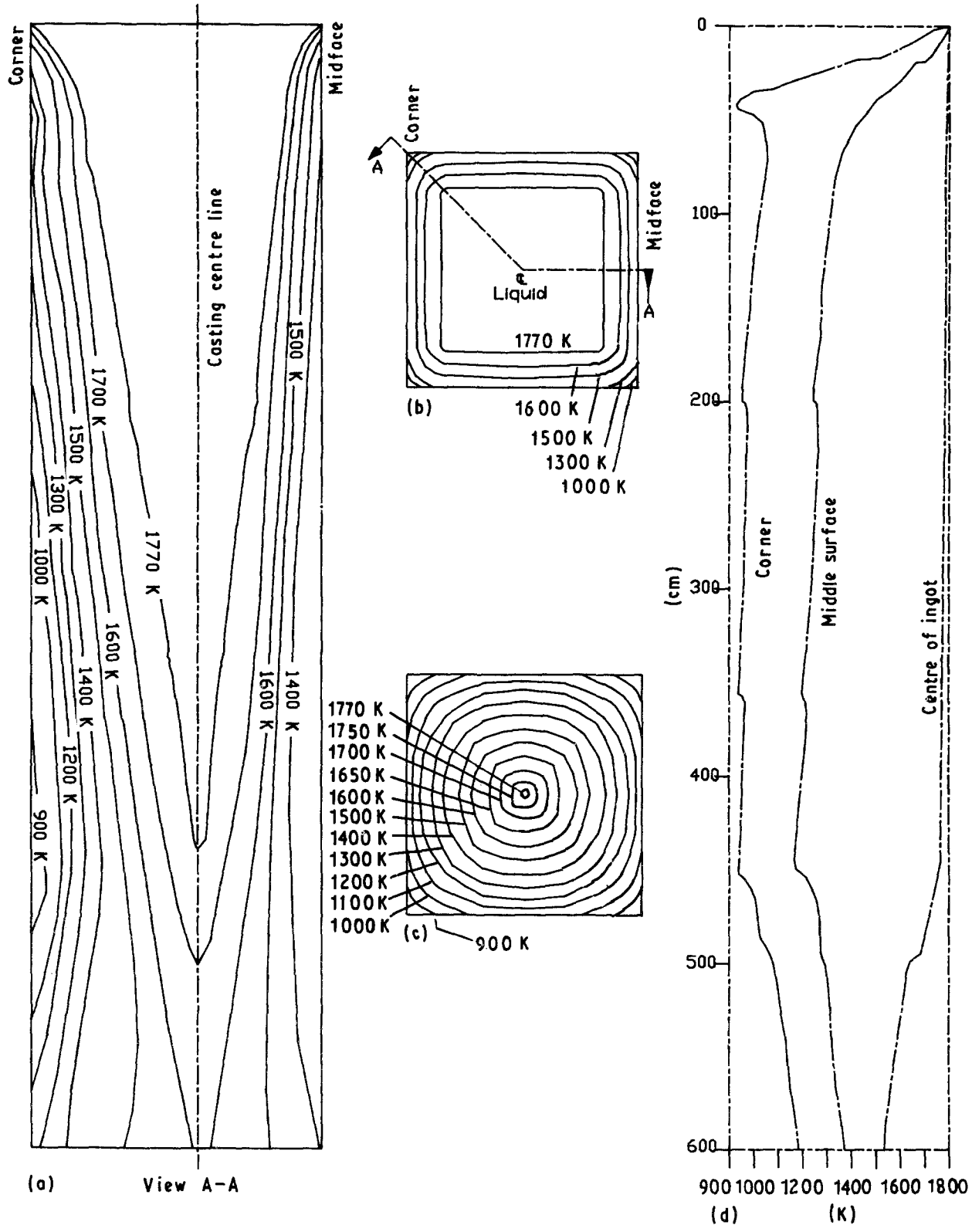

Figure 5 Shell thickness and temperature distribution. (a) Temperature contour lines along casting direction. (b) Temperature contour lines below the mould. (c) Temperature contour lines near complete solidification. (d) Temperature distribution along casting direction.

of these types of problems. The relative ratio of the calculated stress to yield stress may interpret the complex deformation resulting from mechanical or thermal stresses and consequential internal and surface cracking of the ingot.

5. Results

A typical 15 cm by 15 cm square section of ingot was selected as an example for analysis. Owing to symmetry, only one-eight of the section has been considered for thermal analysis. The temperature distributions within the ingot, Fig. 5, show that the corner points are experiencing the maximum thermal variation (whenever there is a change in the boundary state). The centre of the casting has almost no temperature change until the last drop of liquid metal solidifies and then the centre temperature decreases rapidly.

The ratio of the calculated Von-Mises stress (due to

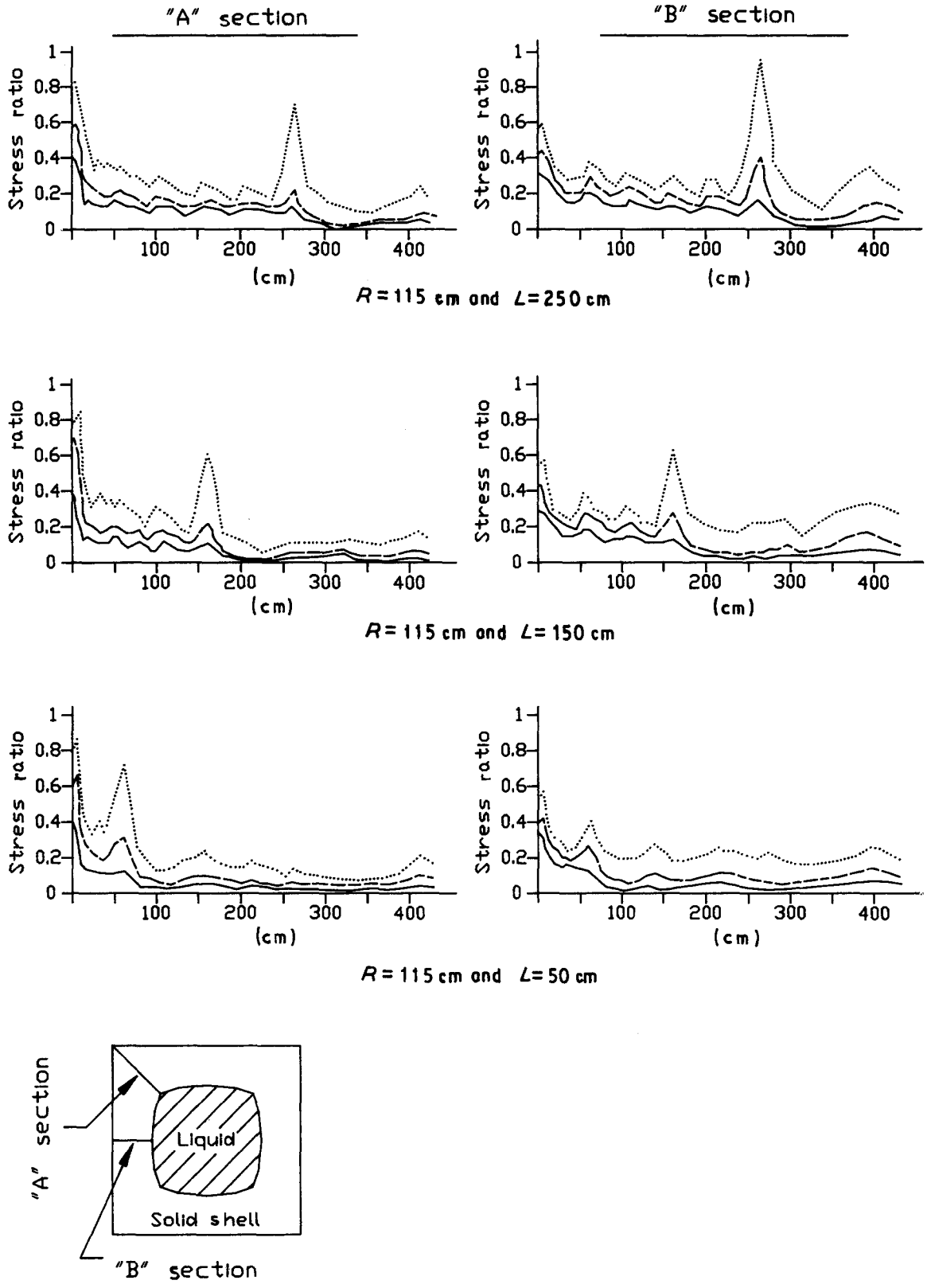

Figure 6 Stress ratios along the casting direction: (. . . .) near the solidification front; (– – –) midway, (——) surface. R = radius of curved portion, L = location of bending rollers.

thermal and mechanical stresses) to the yield stress was considered as a basis for the possibility of cracking. Any location with a high stress ratio has a greater chance of cracking. Fig. 6 shows the typical stress ratios, resulting from the stress analysis. The stresses must be considered for at least a quarter of the ingot section because some of the external forces are being applied on only one side of the casting.

The results of the calculated stress ratio, using the theory of elasticity, show that the possibility of crack formation is in the same location as others experimentally determined [13] and previously published [2]. Based on these confirming results, by assuming various values for the involved parameters, the computer program for stress analysis has been executed many times. The results can be interpreted as follows.

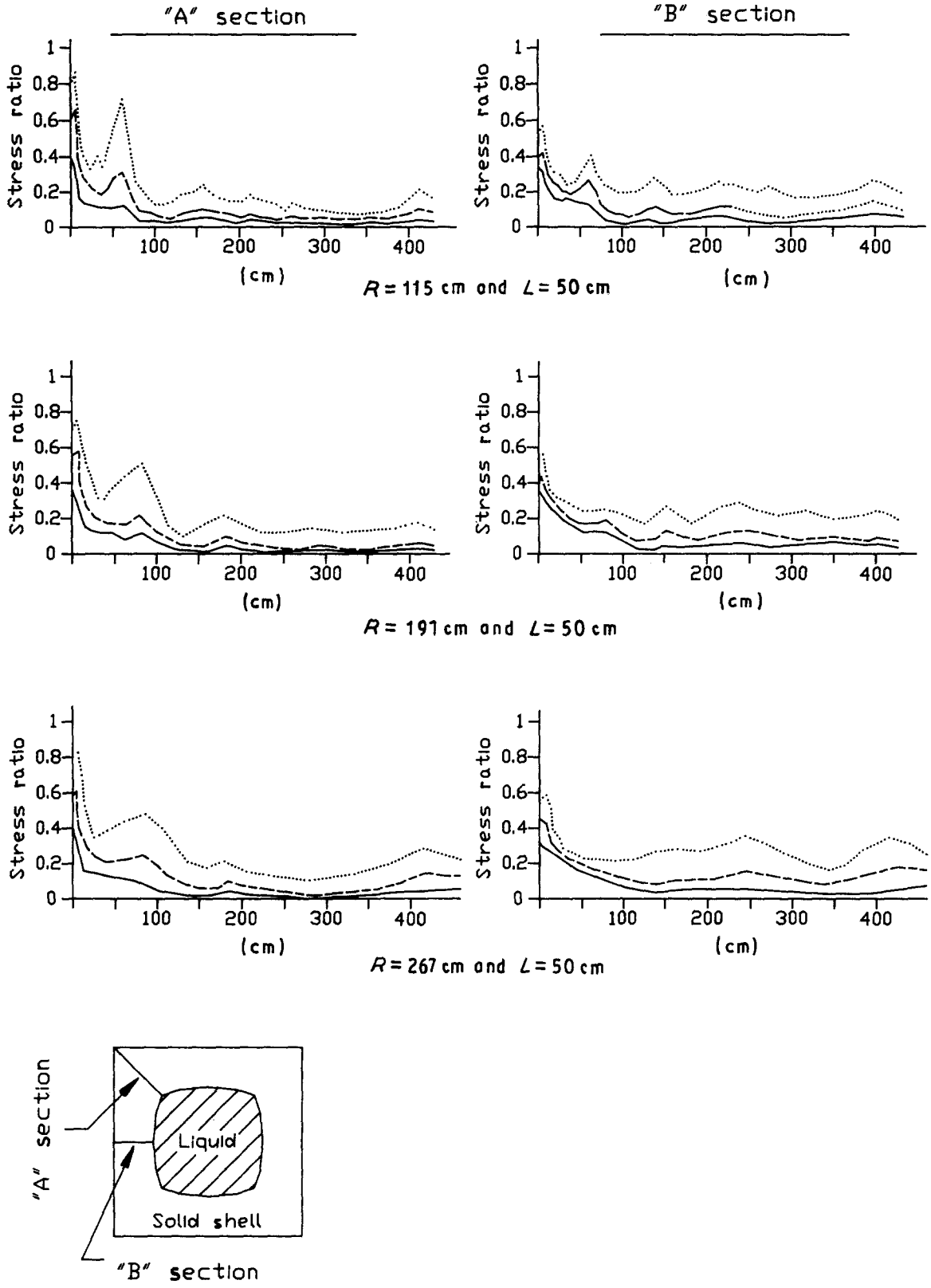

Figure 7 Stress ratios along the casting direction. For key, see Fig. 6.

5.1. Thermal stress problems

The high stress ratio is observed in Section A, between 0 and 20 cm below the mould, rather than Section B. The surface temperature, in the corner of the ingot (A face), has increased approximately 170 K. This dramatic temperature change, which causes higher stress ratios, is due to the changing heat-transfer coefficient in the mould and spray water cooling methods. Cracks reportedly occurred in these locations and were observed experimentally [13]. The complete solidification also leads to a sharp drop in the centre temperature and a small increase in the stress ratio of the ingot.

5.2. Mechanical stress problems

The location of the bending roller was varied from 50–400 cm below the mould and the radius of curvature was increased from 76 cm to 344 cm. The first consideration is the location of the bending rollers, as

a higher stress ratio develops when these rollers are located far from the mould, Fig. 6. The pinch rollers and straighteners may also cause partial cracks when the bending rollers are too close to the mould. The pinch rollers, if located far from the mould, are more likely to cause surface cracks.

A second consideration is the radius of curvature, because the results, see Fig. 7, indicate that a higher radius decreases the stress ratio at the location of the bending rollers. A lower curvature radius requires the bending rollers to force more radial displacement of the casting. The higher radius also decreases the risk of surface and mid-way cracking at the location of the bending rollers. Finally, if the radius and location of the curved portions are considered, the risk of crack formation would be lowest when the curve is closest to the mould or after complete solidification. In either case the radius must be as large as possible.

Based on the numerical results the vertical type of continuous casting produces the least risk to crack formation. From an economic point of view, the vertical casting type is not a suitable choice, because it requires new buildings and an installation of a high crane. The Arc type of continuous casting with bending provides minor risk to crack formation, because the bending process is initiated at the very beginning of solidification. The Arc method, with curved mould, is capable of providing a very large radius of curvature which further decreases crack formation.

6. Conclusions

The numerical model developed is capable of calculating an approximation of the temperature and stress distribution in a continuous casting. Owing to the lack of information on the mechanical properties of steel at high temperatures and other control variables, the stress ratios obtained have a limited value. The experimental data for material properties and applied forces are limited but it is possible to predict the regions which have the potential to cause cracks. Based on the numerical results obtained, the most ideal continuous casting process which produces the least risk to crack formation is the Arc type with a curved mould.

References

1. R. W. JOSEPH and N. T. MILLS, "A look inside strand cast slabs" (AISE, New York, 1975).
2. J. K. LAIT, J. K. BRIMACOMBE and F. WEINBERG, *Iron Making Steel Making* **1** (1974) 90.
3. T. INOUE and Z. G. WANG, *Ingenieur Archiv* **58** (1988) 265.
4. B. C. RAYCHAUPHURI, *Mech. Engng Bull.* (1977) 51.
5. J. MATHEW and H. D. BRODY, in "International Conference on Computer Simulation for Material Application: Proceedings" (1976) 1138.
6. A. I. MANESH, *J. Mater. Shaping Technol.* **8** (3) (1990) 179.
7. L. J. SEGERLIND, "Applied Finite Element Analysis" (Wiley, 1983).
8. J. E. KELLY, K. P. MICHALEK, T. G. O'CONNOR, B. G. THOMAS and J. A. DANTZIG, *Metall. Trans.* **19A** (1988) 2589.
9. R. D. PEHLKE, "Modeling of heat Transfer and Solidification in Continuous Casting of Steel", NTIS-PB83-2110033 (University of Michigan, USA, 1982) p. 7.
10. E. A. MIZIKAR, *Iron Steel Eng.* **47** (1970) 53.
11. A. I. KOLER, J. D. THOMAS and A. A. TZARARAS, *Cast Metal Res. J.* (1973) 156.
12. G. A. FISCHER, *Proc. ASTM* (1970) 1137.
13. A. GRILL, J. K. BRIMACOMBE and F. WEINBERG, *Iron Making Steel Making* **3** (1976) 38.

Received 4 April
and accepted 30 July 1991